JOURNAL OF PROPULSION AND POWER
Vol. 22, No. 4, July–August 2006

Numerical Simulation of Three-Dimensional Reacting Flow in a Model Supersonic Combustor

A. Rajasekaran* and V. Babu†
Indian Institute of Technology, Madras 600 036, India

Numerical simulations of the three-dimensional reacting flow in a staged supersonic combustor (Mach 2.5) have been carried out. The combustor has a strut for the first stage and wall-mounted injectors for the second stage (S. Tomioka, A. Murakami, K. Kudo, and T. Mitani, "Combustion Tests of a Staged Supersonic Combustor with a Strut," *Journal of Propulsion and Power*, Vol. 17, No. 2, 2001, pp. 293–300). The Spalart–Allmaras model has been used for modeling turbulence and single-step finite-rate chemistry has been used for modeling the H_2/Air kinetics. The grid has been refined to achieve average value for wall y^+ less than 20. The predicted static-pressure profile along the centerline of the combustor is compared with experimental data for different injection schemes. Details of the flowfield inside the combustor as well as variation of mixing efficiency, combustion efficiency, and total pressure loss along the length are presented and discussed.

Nomenclature

A	=	cross-sectional area of the combustor, m^2
$\dot{m}_{\text{fuel,in}}$	=	mass flow rate of fuel, kg/s
P	=	static pressure, Pa
P_0	=	local stagnation pressure, Pa
$P_{0,\text{inlet}}$	=	inlet stagnation pressure, Pa
T	=	static temperature, K
T_0	=	local stagnation temperature, K
$T_{0,\text{inlet}}$	=	inlet stagnation temperature, K
u	=	velocity along the x direction, m/s
α	=	local fuel mass fraction
α_s	=	stoichiometric fuel mass fraction
γ	=	ratio of specific heats
η_c	=	combustion efficiency
η_m	=	mixing efficiency
η_t	=	total pressure loss
ρ	=	mass density, kg/m^3
ϕ	=	local equivalence ratio

Introduction

INTEREST in hypersonic technology has initiated intense research in supersonic combustors. The design of fuel injection and flame-holding mechanism plays a very important role in the performance of a supersonic combustor. The efficient mixing of fuel and air is difficult to achieve in a supersonic combustor because of short flow residence times, typically of the order of few milliseconds. To achieve increased penetration and better mixing, different fuel injection and mixing enhancement techniques are used. An excellent review of these techniques has been given by Bogdanoff.[1] These include injection through holes on the combustor wall, injection through slots parallel to the flow, and injection from struts and ramps. The promise of advanced mixing techniques such as a curved combustor where the buoyancy forces aid the penetration of the fuel across the combustor, increased pulsation of fuel injectors to increase the penetration, and mixing and injection behind pylons to allow deep penetration are also assessed in his work.

Received 6 December 2004; revision received 9 June 2005; accepted for publication 19 June 2005. Copyright © 2005 by V. Babu. Published by the American Institute of Aeronautics and Astronautics, Inc., with permission. Copies of this paper may be made for personal or internal use, on condition that the copier pay the $10.00 per-copy fee to the Copyright Clearance Center, Inc., 222 Rosewood Drive, Danvers, MA 01923; include the code 0748-4658/06 $10.00 in correspondence with the CCC.

*Ph.D Student, Department of Mechanical Engineering.
†Associate Professor, Department of Mechanical Engineering; vbabu@iitm.ac.in.

As reported by Papamoschou and Roshko,[2] mixing is effected by the reduction in mixing-layer growth in high-speed flow. The growth rate directly depends on the convective Mach number, which is derived based on the difference in speed between the fluid and acoustic speed; this further affects the design of an efficient fuel-injection system.

It appears from the work of Marble et al.[3] that the fuel jet path should be designed so as to intersect the shocks from the surfaces ahead of the fuel-injection zone, to enhance mixing. The presence of a baroclinic torque in hydrogen jets, caused by a shock intersecting the jet, is brought out in their work. This leads to a pressure gradient normal to the density gradient, which helps in creating vortices that enhance the mixing rate substantially.

Brandstetter et al.[4] conducted experimental investigations with special attention to flame stabilization and operation over a wide range of flight Mach numbers. The combustion chamber entry Mach number was varied between 1.7 and 2.1 and the stagnation temperatures between 500 and 1200 K, in order to be near the transition point from ramjet to scramjet operation. Experimental results for two different injection systems, namely, ramp injection and a more promising strut injection, are presented in their work.

Tomioka et al.[5] designed a staged supersonic combustor model with a strut for the first stage and wall-mounted injectors for the second stage to avoid combustor-inlet interaction. The staged supersonic combustor was tested for Mach 2.5 airflow with a total temperature of 1500 K. With staged injection, the pressure rise caused by first-stage combustion was isolated from that of the second-stage combustion, and fuel with an equivalence ratio of more than unity could be injected without causing separation in the inlet section. The maximum thrust increment was augmented by 100% when compared with first-stage injection alone. Second-stage injection further upstream resulted in slightly higher thrust, but resulted in separation penetration at higher fuel flow rates.

Yu et al.[6] carried out supersonic H_2/air combustion experiments for a fixed-entry Mach number 2.5 using eight different model combustors, at various stagnation conditions and global equivalence ratios. Specifically, the stagnation temperature was varied from 1200 to 2000 K, stagnation pressure from 1 to 1.4 MPa, and the global equivalence ratio from lean to rich. Effects of wall injection, strut injection, and cavity flame holder were systematically investigated and compared. Yu et al.[7] carried out experimental investigations on the ignition and combustion stabilization of kerosene with pilot hydrogen in Mach 2.5 airflows using two test combustors, with cross sections of 30.5×30 and 51×70 mm, respectively. Various integrated modules, including the combinations of different pilot injection schemes and recessed cavity flame holders with different geometries, were tested.

Very little has been reported in the open literature on the numerical simulation of the reacting flow in supersonic combustors. Kim et al.[8] reported a two-dimensional numerical study on supersonic combustion with cavity-based fuel injection. The effect of varying cavity aft wall angle, offset ratio of upstream to downstream depth, and cavity length on hydrogen injection into the supersonic air flow was investigated. The cavity was found to enhance combustion efficiency, but it also increased the total pressure loss.

Rodriguez and Cutler[9] carried out a three-dimensional numerical analysis in a SCHOLAR supersonic combustor using the VULCAN code. In this combustor, hydrogen is injected at an angle of 30 deg from the wall into a Mach 2.5 supersonic airstream. The effect of turbulence parameters such as Schmidt number, Prandtl number, and inflow turbulence in the reacting flow solution is studied. The numerical solutions were found to be sensitive to the type of turbulence model and the inflow turbulence parameters used. The difficulty in accurately predicting the ignition delay time, combustion pressure rise, and fuel plume penetration is discussed, but no clear modeling method to predict all of the three parameters with a reasonable accuracy is reported.

Oevermann[10] presented a numerical method for the simulation of turbulent diffusion flames using the flamelet approach in two-dimensional compressible flows. This method has been used for numerically investigating the combustion of hydrogen in a supersonic airstream. Although the calculations were viscous, no-slip boundary condition is not implemented on the walls. The numerical results are compared with experimental data, and the differences between the two are attributed to the slip boundary condition used in the numerical study as well as significant three-dimensional effects in the experiments. In this context, it is also mentioned that the validity of the flamelet approach to supersonic combustion still remained to be established.

In this paper, results from three-dimensional numerical simulations of the reacting flow in a staged supersonic combustor are presented. The geometry considered in the present work is the same as the one studied experimentally by Tomioka et al.[5] The simulations have been performed using the commercial software FLUENT.[11]

Computational Methodology

The model supersonic combustor considered in the present work is shown in Fig. 1. Vitiated air enters through the inlet, with hydrogen being injected through the strut as well as from the walls depending upon the type of configuration. The injection ports on the strut are not shown in the figure for the sake of clarity. In the present work, vitiated air (mass fraction of O_2, H_2O, and N_2 being 0.198, 0.139, and 0.663, respectively) enters the combustor at a Mach number of 2.5 and a stagnation temperature and pressure of 1500 K and 1 MPa. The inlet conditions of the H_2 injection ports are adjusted so as to achieve sonic injection with the desired fuel mass flow rate. The flow through the combustor is compressible and three dimensional. In addition, turbulence and finite-rate chemistry also have to be considered.

In this work, the Spalart–Allmaras model with default values for the model constants ($C_{b1} = 0.1355$, $C_{b2} = 0.622$, $C_{v1} = 7.1$, $C_{w2} = 0.3$) has been used for modeling turbulence. The turbulent Schmidt number has been taken to be 0.7. The Spalart–Allmaras model is a relatively simple one-equation model that solves a modeled transport equation for the kinematic eddy (turbulent) viscosity. In this model, it is not necessary to calculate a length scale related to the local shear-layer thickness. It is designed specifically for aerospace applications involving wall-bounded flows and has been shown to give good results for boundary layers subjected to adverse pressure gradients. For three-dimensional flows, the use of a one-equation model over two-equation models can result in considerable savings in computational effort. However, this model is known to have difficulties in predicting free shear flows, and its suitability to these types of flows has not been clearly established. In this context, it is also important to bear in mind the sensitivity of RANS calculations to the values used for turbulent Schmidt and Prandtl numbers as demonstrated clearly by Baurle[12] and Baurle and Eklund.[13]

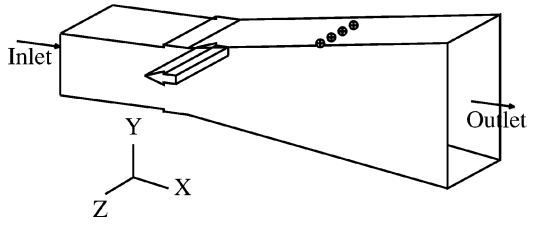

Fig. 1 Schematic of the model combustor.[5]

Single-step finite-rate kinetics has been used to model chemistry. Rate data for the $H_2 - O_2$ forward reaction mechanism have been taken from Hsu and Jemcov.[14] Backward rates are calculated based on the equilibrium constant. Viscosity and C_p of the mixture have been evaluated using mass-weighted-mixing law. For the individual fluids in the mixture, these properties have been evaluated using Sutherland's law and fifth-order polynomials in temperature, respectively.

Although the full geometry is shown in Fig. 1, calculations have been carried out in quarter geometry as the flowfield can be considered to be symmetric about the horizontal and the vertical midplanes. This results in considerable savings in computational effort. Adiabatic boundary conditions along with standard wall functions have been used on all of the wall surfaces. At the air inlet where the flow is supersonic, pressure inlet conditions, namely, stagnation and static pressure, stagnation temperature, and species mass fraction are specified. In addition, inlet turbulence intensity and the hydraulic diameter have been specified. At the hydrogen inlet, where the flow is sonic, mass-flow inlet conditions, namely, mass-flow rate of hydrogen, static pressure, total temperature, and species mass fraction are specified. All of the flow variables at the outlet boundary including pressure are determined from the interior of the domain by extrapolation.

The three-dimensional numerical simulations have been carried out using the commercial software FLUENT. The coupled solver available in FLUENT has been used with explicit time stepping. All of the calculations have been carried out using second-order-accurate discretization.

Numerical solutions to the problem just outlined but without H_2 injection were obtained on an initial tetrahedral/hybrid grid with 254,658 cells. This grid was then refined successfully. Firstly, adaption based on gradients of static pressure was done, so that the shocks could be captured accurately. Secondly, refinement near all of the no-slip surfaces was done so as to resolve the boundary layers well and to achieve wall y^+ values as low as possible. This refinement resulted in grids with 309,220 and 362,385 cells. The maximum values of wall y^+ for the three grids are approximately 228, 165, and 118, respectively. Static-pressure distribution along the sidewall on different grids showed that although the coarse and intermediate grid results are quiet close to that of the fine grid in most places; the fine-grid results are better resolved in the vicinity of the reflected shocks. The grid with 362,385 cells is adequately able to resolve the flowfield, and all of the nonreacting flow solutions have been obtained on this grid.

For reacting flow calculations the grid is adapted further based on the gradients of reacting species so as to resolve the combustion phenomenon in the flowfield accurately. After progressive refinement, a grid with 751,690 cells has been taken as the final grid for all subsequent calculations. The maximum value of wall y^+ on this grid is 50, while the area-averaged value is below 20. These details are summarized in Table 1. In this context, the following points should be kept in mind. For turbulent calculations such as the present one, wall y^+ values less than 100 are generally acceptable.[9] However, the use of standard wall functions in the simulations requires that the wall y^+ values be below 30, so that the cell closest to the wall can be safely said to be inside the log-law region. In flows with shocks, it is not always possible or feasible to get the wall y^+ value below 30 *everywhere*, especially at the points of impingement and reflection of shocks. So the area-averaged wall y^+ can be used as a companion metric for such flows. Furthermore, global (overall) mass conservation is also important, and for all of the results reported here the

Table 1 Grid-independence study

Discretization	No. of cells	Wall y^+ Max	Wall y^+ Avg
Nonreacting flow (no fuel)			
Baseline grid	254,628	228	——
First adaption	309,220	165	112
Second adaption	362,385	118	90
Strut injection			
Nonreacting flow	751,690	37	17
Reacting flow	751,690	37	18
Strut+wall injection			
Nonreacting flow	751,690	55	17
Reacting flow	751,690	42	17
Wall injection			
Nonreacting flow	751,690	40	16
Reacting flow	751,690	61	9.8

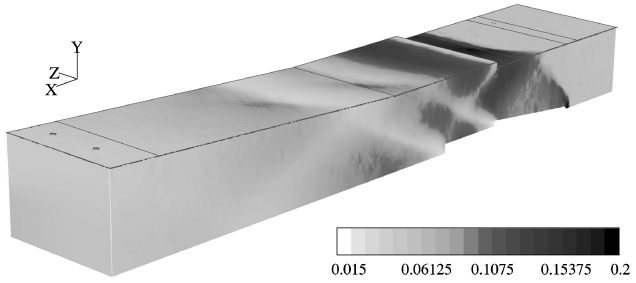

Fig. 2 Contours of dimensionless static pressure on the side and top wall (no fuel).

difference in mass between inlet(s) and outlet is about 10^{-6} kg/s. The integrated value of the fuel mass-flow rate for nonreacting and reacting flow at various $x =$ constant sections downstream of the injection locations is within 1–2% of the injected fuel mass-flow rate. This serves as a check on global fuel conservation and is also an important metric.[15]

Results and Discussion

Numerical solutions have been obtained for both the nonreacting and reacting flows with three injection schemes—strut, strut+wall, and wall injection. In addition, the flowfield in the absence of any fuel injection is also presented. All of the results presented correspond to the top-right quadrant of the geometry shown in Fig. 1.

No Fuel Injection

The contours of static pressure (nondimensionalized with inlet stagnation pressure) on the side and top wall are shown in Fig. 2. The oblique shock from the leading edge of the strut and the expansion fan at the shoulder and at the base can be seen clearly in Fig. 2. In addition, the expansion fan from the corner of the step on the combustor wall and the pressure rise caused by the reattachment shock on the top wall just past the step are also seen. The reflection of the leading-edge oblique shock from the top wall impinges on the strut just past the shoulder and quite close to the reattachment line of the separated flow on the shoulder. The reflection of this shock merges with the reattachment shock and an oblique shock of almost the same strength as the incident shock emerges from this region. There is also a reattachment shock because of the separated flow at the base of the strut. Both of these shocks impinge on the top wall but are not reflected back with any significant strength because of flow expansion caused by the divergence of the top wall.

Thrust force can be obtained as the difference in the integrated value of the impulse function at the exit and the inlet, that is to say,

$$\mathcal{T} = \left(\int p \, \mathrm{d}A + \int \rho u^2 \, \mathrm{d}A \right)_{\text{inlet}}^{\text{exit}}$$

For this case where there is no fuel injection, the thrust force (for the quarter geometry) comes out to be 10.35 N. Using this as the baseline value, the thrust increment caused by combustion can be calculated for all of the other cases. Mass-averaged values of pressure, temperature (nondimensionalized with inlet stagnation conditions), Mach number, and γ at the exit plane for all of the configurations are given in Table 2. (Tomioka et al.[5] measured pitot pressure and gas composition at the exit plane, and all of the other properties were estimated using equilibrium and quasi-one-dimensional calculations.) It can be seen that the loss of total pressure is as high as 56% for this case even in the absence of combustion. This is the consequence of the presence of the strut in the flow. Cavity-based combustors that do not use a strut for injection have lower stagnation pressure losses.[8,15]

Table 2 Mass-averaged values for properties at the exit plane

Source	Mach number	Pressure Static	Pressure Total	Static Temp.	γ
Baseline (no fuel)					
Present	2.275	0.03	0.4473	0.556	1.331
Strut injection					
Present	1.77	0.0533	0.322	1.0	1.28
Expt[5]	1.83	0.05	0.29	0.99	1.28
Strut+wall injection					
Present	1.386	0.085	0.273	1.333	1.25
Expt[5]	1.31	0.092	0.24	1.39	1.25
Wall injection					
Present	1.36	0.087	0.271	1.186	1.265
Expt[5]	1.21	0.094	0.22	1.43	1.25

Strut Injection

Injection of H_2 through the ports in the strut results in a bow shock just ahead of the ports. The consequence of this pressure rise is to make the separated flow region on the strut bigger. The flow structure near the injection port is very similar to the one outlined by von Lavante et al.[16] and Baurle et al.[15] The general nature of the flowfield everywhere else is the same as the previous case.

Figure 3a shows contours of dimensionless pressure with combustion taking place. The rise in pressure caused by combustion completely cancels the expansion around the strut shoulder. The higher pressure also results in the separation zone on the strut becoming larger in the region between the injection ports. Contours of static pressure on the strut surface (Fig. 3b) show the footprints of the bow shock and the reattachment shock. The large separation zone on the strut surface as well behind it helps to trap the fuel and stabilize the combustion process. The separated region on the strut surface ahead of and behind the injection port is shown in Fig. 3c.

The thrust developed for this case comes out to be 96.7 N. The exit Mach number is 1.77, which indicates that further heat addition is possible. There is an additional 12% loss of stagnation pressure caused by combustion with a doubling of the exit static temperature compared with the baseline case without fuel injection. The fuel injection itself contributes very little to the loss of stagnation pressure. The presence of the additional water vapor at the exit caused by combustion lowers the molecular weight of the mixture[17] as well as γ. The value for γ decreases from 1.34 for the baseline case to 1.28 for this case.

Strut+Wall Injection

The flowfield in this case shows some interesting features in the neighborhood of the wall-injection ports (Fig. 4a). This figure shows a bow shock upstream of the injected fuel jet and V-shaped expansion fans just downstream on the top wall, in the absence of combustion. In addition, a reattachment shock just after the expansion fan is also seen. The expansion fan and the reattachment shock are generated as the flow divides to flow around the separation region downstream of the jet and then rejoins.

Contours of static pressure with combustion taking place, are shown in Fig. 4b. The pressure rise caused by combustion in the strut region is almost identical to that shown in Fig. 3a. This is to

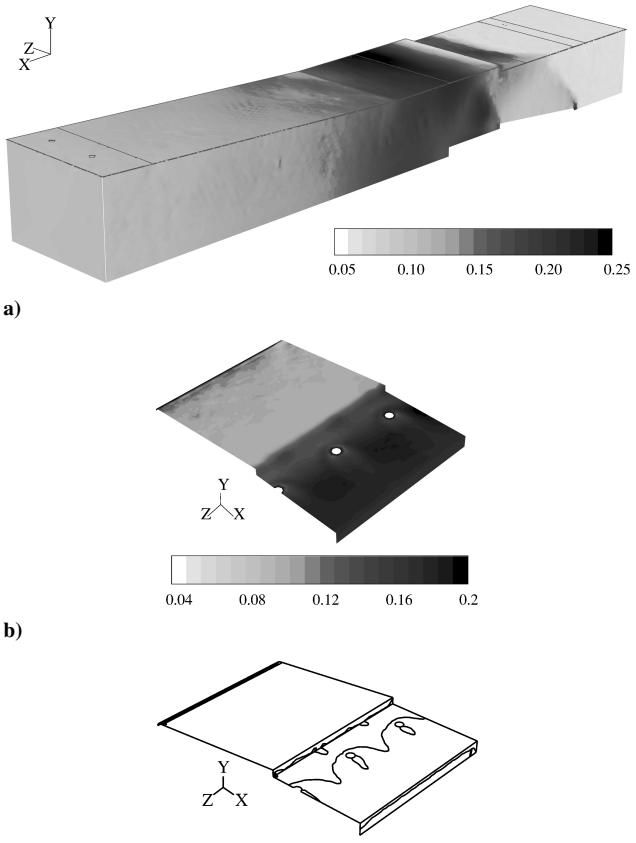

Fig. 3 Fuel injection from the strut ($\phi = 0.34$)—reacting flow. Contours of dimensionless static pressure on the side and a) top wall and b) strut surface and c) outline of separated flow on the strut surface.

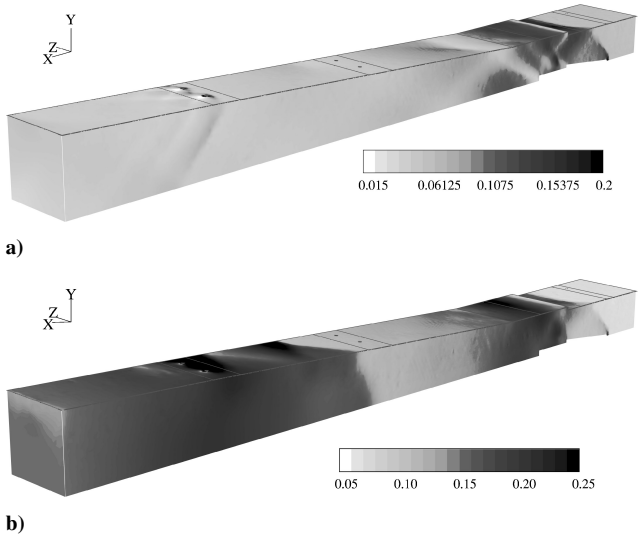

Fig. 4 Fuel injection from strut ($\phi = 0.44$) and from the wall ($\phi = 0.61$). Contours of dimensionless static pressure on the side and top wall a) nonreacting and b) reacting.

be expected as the amount of fuel injected through the strut is more or less the same between these two cases. However, the flowfield in the diverging part of the combustor is radically different. As can be seen in Fig. 4b, combustion actually starts upstream of the wall-injection ports. This is because of the rapid diffusion of H_2 in the upstream direction from the injection point and the availability of O_2 at elevated temperatures as a consequence of the combustion near the strut. Although the amount of fuel injected through the wall is higher than that through the strut, combustion is nearly complete within a very short distance downstream of the wall-injection port.

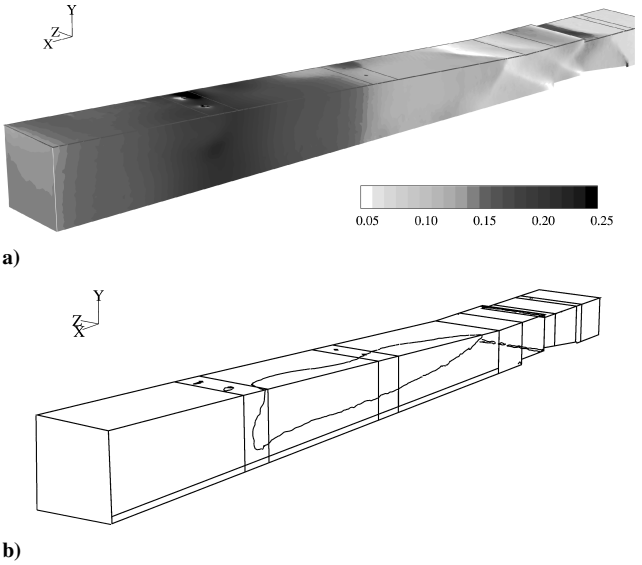

Fig. 5 Fuel injection from the wall ($\phi = 0.94$): a) contours of dimensionless static pressure on the side and top wall (reacting) and b) outline of separated flow on the side and top wall.

The thrust force for this injection scheme is calculated to be 181.86 N, and the average Mach number at the exit is 1.386. The higher thrust and the lower Mach number can be attributed to the combustion of the additional fuel injected through the wall. The total pressure loss is also 17% higher than the baseline case. The value for γ for this case is 1.25, which is less than the value for strut-injection case, owing to the combustion of additional amount of H_2 giving rise to more water vapor.

There is no flow separation on the wall surface downstream of the step despite the pressure rise caused by combustion near the wall-injection region. This indicates that the initial pressure rise as a result of combustion in the strut region is sufficient to overcome the adverse pressure gradient downstream. It is reasonable to surmise that more fuel can be injected at the same wall location or further downstream.

Wall Injection

Contours of dimensionless static pressure on the side and top wall for the reacting flow are given in Fig. 5a. It can be seen that the expansion fan from the strut step and the base are stronger now than in the previous two cases. This is because of the absence of fuel injection in the strut and the attendant bow shock. The region of high pressure, which, so far, had shown symmetry about the injection ports, now is completely shifted towards the symmetry plane. There is hardly any combustion taking place near the injector closer to the side wall. The reason for this is the massive flow separation upstream of the wall-injection ports in response to the pressure rise caused by combustion. The outline of the separated region on the side and top walls is shown in Fig. 5b. Flow separation begins almost after the step on the combustor wall and extends almost up to the injection point. The consequent separation shock on the combustor top and side wall can be seen clearly in Fig. 5a.

The thrust developed is 145.01 N, which is lower than the previous case, despite the same amount of fuel being injected ($\phi = 0.91$). The value for the nondimensional static temperature at the exit plane, 1.186 given in Table 2, is also less than the corresponding value for the previous case. This is a clear indication that the mixing and combustion are poor in this injection scheme.

Overall Performance Measures

In this section, some one-dimensional metrics for assessing the overall performance of the combustor are discussed. The desired objectives in a supersonic combustor are proper mixing of the fuel and

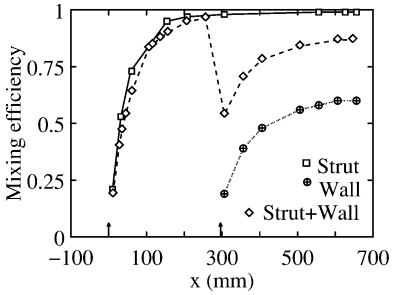

Fig. 6 Variation of mixing efficiency for the three injection schemes.

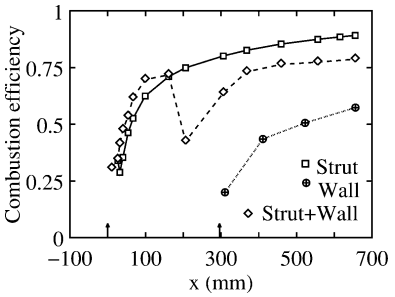

Fig. 7 Variation of combustion efficiency for the three injection schemes.

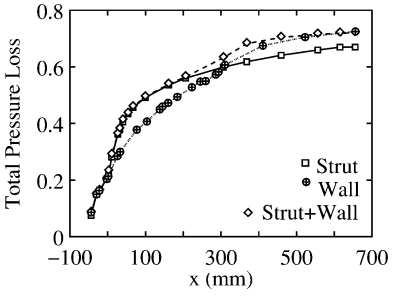

Fig. 8 Variation of total pressure loss for the three injection schemes.

air, complete combustion of the fuel, and minimal loss of stagnation pressure. The level of mixing in a particular combustor design can be determined by defining a mixing efficiency that will be high wherever the fuel and oxygen are in stoichiometric proportion. Following Baurle et al.,[15] the mixing efficiency at a $x =$ constant section can be defined as

$$\eta_m = \frac{\int_x \alpha_R \rho u \, \mathrm{d}A}{\sum_x \dot{m}_{\text{fuel,in}}}$$

The denominator represents the total amount of fuel injected upstream of this section. The quantity α_R in the numerator is given as[15]

$$\alpha_R = \begin{cases} \alpha, & \alpha \leq \alpha_s \\ \alpha_s \dfrac{1-\alpha}{1-\alpha_s}, & \alpha > \alpha_s \end{cases}$$

Variation of the mixing efficiency (nonreacting flow) for the three injection schemes is given in Fig. 6. In all of the three cases, a steep increase in the mixing efficiency can be seen downstream of the injector, as the fuel mixes rapidly with the main flow. The strut-injection scheme shows high mixing efficiency (almost equal to 1) because the global equivalence ratio is only 0.34. The strut+wall injection scheme shows higher values of mixing efficiency near the strut region, but the profile flattens out and then decreases sharply before the wall-injection port. This is because of extra fuel being available as a result of diffusion from the wall-injection region. The wall-injection scheme shows the poorest performance of the three injection schemes with a maximum value of 0.6 for the mixing efficiency. As pointed out by Baurle et al.,[15] this means that only 60% of the fuel is likely to burn under stoichiometric condition. Mixing is poor in this case primarily because of the shorter residence time. Combustion efficiency at a given $x =$ constant section is a measure of how much of the fuel injected upstream has been consumed at that station. This can be written as

$$\eta_c = 1 - \frac{\int_x \alpha \rho u \, \mathrm{d}A}{\sum_x \dot{m}_{\text{fuel,in}}}$$

Variation of combustion efficiency given in Fig. 7 shows the trends to be almost the same as that of the mixing efficiency. The strut-injection scheme is the most efficient with an asymptotic value of 0.892. This is to be expected because there is more time available for the fuel to be consumed in this case and the amount of fuel injected is also the least. The strut+wall injection scheme shows a maximum combustion efficiency of 0.787. Injection from the wall alone shows poor efficiency throughout likely because of the large separation bubble on the walls upstream of the injector, which occupies a considerable portion of the cross section and the fact that there is no recirculation zone downstream to provide flame holding. The maximum efficiency achieved for this case is only 0.57.

Total pressure loss is defined as[15]

$$\eta_t = 1 - \frac{\int_x P_0 \rho u \, \mathrm{d}A}{\int_x P_{0,\text{inlet}} \rho u \, \mathrm{d}A}$$

This is plotted in Fig. 8 for the three injection schemes. Sharp increase in total pressure losses is seen at the nose of the strut ($x = -43$ mm). The strut and the strut+wall injection scheme show identical trends until the wall-injection location, beyond which the latter exhibits higher loss of total pressure caused by combustion of the fuel injected from the wall. The total pressure loss in the wall-injection scheme is initially lower but increases in the region where combustion is taking place. As the fuel is being injected into a higher-Mach-number flow in this case, the loss of total pressure is higher, and so the total pressure loss at the exit comes out to be the same as the strut+wall injection scheme. Because the amount of fuel injected is the least in the strut-injection case, total pressure loss as a result of combustion is the lowest for this case.

Comparison with Experimental Data

In this section, numerically predicted values of exit-plane properties as well as the static pressure along the centerline of the top wall of the combustor are compared with experimental values reported by Tomioka et al.[5] It is important to keep the following sources of uncertainty in mind, while comparing the predictions with the experimental results:

1) The walls of the combustor are taken to be perfectly insulated in the simulations. Realistic thermal boundary conditions will definitely allow some heat loss to take place, which will reduce the temperature in the boundary layer. This will have a cascading effect on the other flow properties.

2) The incoming turbulent boundary layer at the inlet has not been taken into account in the simulations. In addition, the inlet turbulence intensity has been assumed to be 10% for all of the simulations. It is not possible to measure this quantity during the experiments.[9] Inlet turbulence intensity will affect the development of the boundary layer along the combustor walls as well as the flowfield in the interior. An excellent discussion of this point is provided by Rodriguez and Cutler.[9] Ideally, if the flow in the nozzle is also simulated, then the uncertainty in the inlet conditions of the combustor can be minimized.

3) The numerical results reported here are steady-state results with fixed inlet conditions. In the experiments, the inlet stagnation temperature was 1500 ± 50 K, and the inlet stagnation pressure was 1 ± 0.03 MPa. All of the reported pressure data were normalized with the inlet stagnation pressure. The location of shocks, separation, reattachment points, as well as locations of heat release, will be

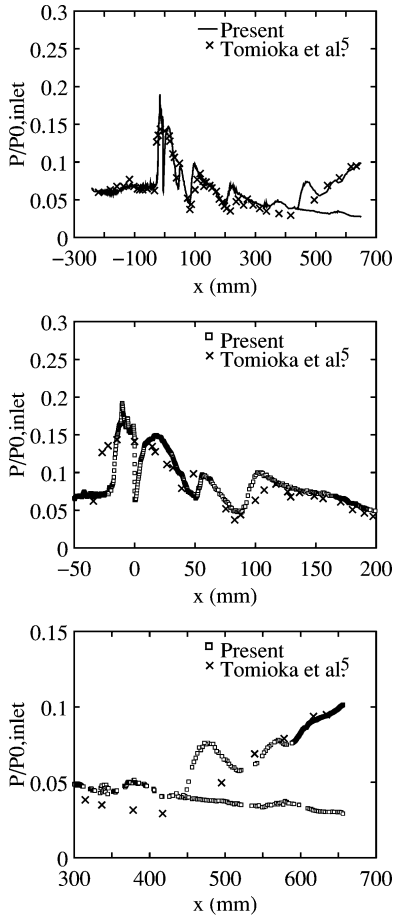

Fig. 9 Comparison of static-pressure distribution along the top wall with experimental data (no fuel).

quite sensitive to variations in the inlet conditions. The extent of this sensitivity during the experiments is not known.

Mass-averaged values at the exit plane are given in Table 2. Of the five properties reported, static and total pressures and static temperature are of primary importance in combustor design. Numerically predicted values of the exit static pressure agree with experimental values to within 8%, whereas there is a maximum difference of 13 and 17% in the values of total pressure and static temperature, respectively. For all of the properties calculated, the maximum difference between predicted and experimental values is seen for the wall-injection case. This is most probably because of unsteadiness in the separated flow that is seen in this case. Nondimensional static-pressure distribution along the centerline of the top wall from the present calculations and from the experiments by Tomioka et al.[5] is given in Fig. 9 for the no-fuel case. In the experiment, there was separation of the flow beyond $x = 400$ mm because of the imposed atmospheric pressure at the exit. Numerical results are shown in Fig. 9 for complete expansion as well as expansion to atmospheric pressure. The trends in the numerical data are quite similar to those seen in the experiments, both in terms of the locations of the shocks/expansion fans as well as their strength. At first sight, it appears as though the pressure rise as a result of the impingement of the oblique shock from the nose of the strut ($x = -43$ mm) and the subsequent pressure drop as a result of the step are overpredicted by the numerical calculations. The same data are shown using an enlarged scale in Fig. 9 in the lower two plots. Careful examination of the experimental data points in this vicinity reveal that the spacing of the pressure taps is too large to pick up the gradients accurately. The separation shock in the divergent portion of the combustor predicted by the numerical simulation is also not seen in the experimental data for the same reason. On the whole, the numerical results are within 10% of the experimental results almost everywhere except near shocks.

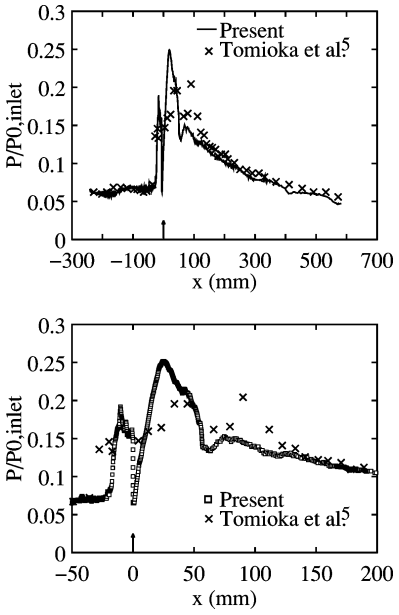

Fig. 10 Comparison of static-pressure distribution along the top wall with experimental data (strut injection).

Static-pressure distribution with fuel injection from the strut is given in Fig. 10. As seen in the enlarged plot in Fig. 10, numerical calculations clearly show the initial pressure rise caused by combustion. But the pressure rise is more than what was reported in the experiments. Although the numerical calculations predict the second pressure rise, the magnitude is underpredicted. As the grid is well refined in this region both in the axial direction as well as in normal direction to the wall, the reason for this discrepancy could be in part caused by the shortcomings of the turbulence model or the single-step kinetics. The agreement between the numerical results and the experimental data beyond $x = 150$ mm is within 5%.

The static-pressure distribution along the centerline of the top wall for the strut+wall injection case is shown in Fig. 11. The pressure rise caused by the combustion of the fuel injected from the strut followed by rapid expansion of the flow is seen clearly in this figure. The modest pressure rise and the gradual expansion of the flow beyond $x = 50$ mm are shown using an expanded scale in Fig. 11. The magnitude of this pressure rise is underpredicted by the numerical calculations. There is a rapid pressure rise following this because of the combustion taking place upstream of the wall injector (around $x = 200$ mm). Numerical results show the location of this pressure rise to be slightly downstream but grossly overpredict the magnitude, when compared with experimental data (third plot in Fig. 11). The latter shows the pressure to be constant, which is somewhat counterintuitive. At about $x = 250$ mm, there is a pressure rise caused by the combustion of the fuel injected from the wall. Once again, the spacing of the pressure taps in the experiment was such that the pressure rise caused by combustion in this region is underpredicted. The agreement between the numerical results and the experimental data is within 5% in the supersonic expansion region beyond $x = 350$ mm.

The static-pressure distribution for the wall-injection case is given in Fig. 12. Figure 5a shows that there are three expansion regions on the top wall—one caused by the step on the wall and two caused by the impingement of the expansion fans from the strut step and the base. As mentioned earlier, these expansions are stronger now than in the previous injection schemes because there is no fuel injection or combustion in this region. These expansion regions are seen clearly in the numerical results shown in Fig. 12, but not in the experimental results. Immediately following the third expansion region is the separation shock caused by flow separation on the side and the top wall (Fig. 5a). The pressure rise resulting from this shock is also seen in Fig. 12 just past $x = 100$ mm. Reflected expansion fan generated upstream (Fig. 5a) results in a decrease in pressure (near

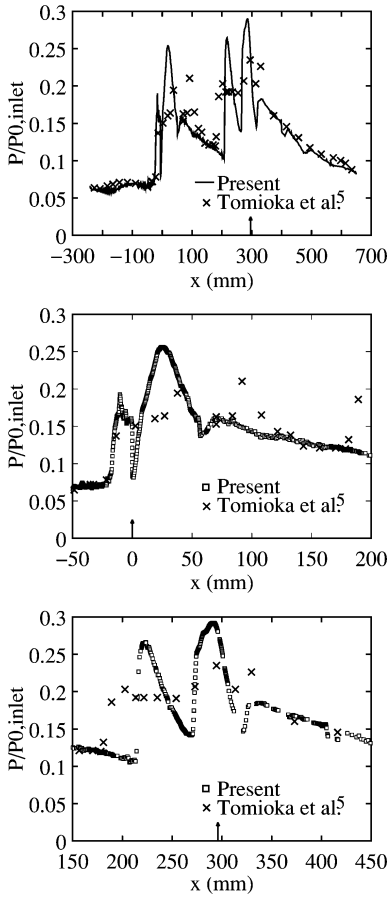

Fig. 11 Comparison of static-pressure distribution along the top wall with experimental data (strut+wall injection).

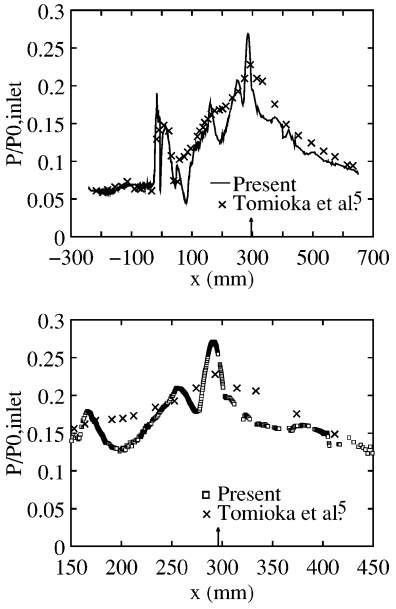

Fig. 12 Comparison of static-pressure distribution along the top wall with experimental data (wall injection).

$x \approx 200$ mm). Experimental data show a steadily increasing profile without any inflection points in this region. Immediately following this region there is an increase in pressure caused by the combustion of the fuel both upstream and downstream of the wall injector. The locations of the pressure rise caused by heat release predicted by the simulations are within 5% of the experimental results. The magnitude of the pressure rise, however, is underpredicted in the experimental data as seen in the enlarged plot in Fig. 12.

The comparison between the numerical and the experimental results for the expanding flow beyond $x = 300$ mm is within 10%. Notwithstanding this, the disagreement between the numerical and experimental profile in the separated flow region is quite evident.

In summary, it can be said that the numerical calculations are able to predict ignition delay, local pressure rise caused by combustion, and overall pressure rise to within 15% for all three injection schemes. The first two are important for determining optimum locations for fuel injection, whereas the last one is essential for determining the thrust.

Conclusions

Numerical simulations of three-dimensional, supersonic combustion in a model combustor incorporating different fuel-injection schemes have been carried out. One-equation Spalart–Allmaras turbulence model and single-step reaction kinetics are used for modeling turbulence and chemistry, respectively. Second-order discretization together with gradient-based adaption and wall y^+ refinement allow the intricate flow details to be captured well. In addition, the resolution of the calculations is such that shock waves/expansion fans not seen in the experimental results are revealed. Comparison of the static-pressure distribution on the top wall of the combustor shows that the numerical predictions are able to capture the trends seen in the experimental data. Mass-averaged values at the exit plane from the numerical calculations compare reasonably well with experimental data.

The staged injection scheme with injection from strut and wall allows more fuel (with ϕ approaching 1) to be burned without significant degradation in mixing, combustion efficiency, or total pressure recovery. Wall injection with $\phi = 0.9$ results in massive flow separation before the injector and consequently shows poor performance.

Although it is quite encouraging to see that with proper resolution numerical simulations are able to predict ignition delay and local as well as overall pressure rise, there are still issues that need to be addressed. These are related to turbulence and chemistry. Comparison of turbulence quantities, temperature, and species distribution inside the combustor are noticeably absent here because these were not reported in the work by Tomioka et al.[5] Of course, the Spalart–Allmaras model that is used in the present work has limitations and cannot predict turbulence quantities such as turbulent kinetic energy.

Use of single-step chemistry is definitely a shortcoming of the present work. As the main objective of the present work was the resolution of the flow scales, single-step finite-rate kinetics was deemed to be adequate for hydrogen combustion. The impact of multistep kinetics on the predicted flowfield is currently being investigated.

Acknowledgments

The authors would like to thank Clayton Rogers and Robert Baurle, Hypersonic Propulsion Branch, NASA Langley Research Center, for providing explanations and insights regarding mixing efficiency. The authors would also like to thank the reviewers for their constructive comments and suggestions.

References

[1]Bogdanoff, D. W., "Advanced Injection and Mixing Techniques for Scramjet Combustors," *Journal of Propulsion and Power*, Vol. 10, No. 2, 1994, pp. 183–190.

[2]Papamoschou, D., and Roshko, A., "The Compressible Turbulent Shear Layer: An Experimental Study," *Journal of Fluid Mechanics*, Vol. 197, 1988, pp. 453–477.

[3]Marble, F. E., Zukoski, E. E., Jacobs, J. W., Hendricks, G. J., and Waitz, I. A., "Shock Enhancement and Control of Hypersonic Mixing and Combustion," AIAA Paper 90-1981, July 1990.

[4]Brandstetter, A., Rocci Denis, S., Kau, H. P., and Rist, D., "Experimental Investigation on Supersonic Combustion with Strut Injection," AIAA Paper 2002-5242, 2002.

[5]Tomioka, S., Murakami, A., Kudo, K., and Mitani, T., "Combustion Tests of a Staged Supersonic Combustor with a Strut," *Journal of Propulsion and Power*, Vol. 17, No. 2, 2001, pp. 293–300.

[6]Yu, G., Li, J. G., Zhang, X. Y., Chen, L. H., Han, B., and Sung, C. J., "Experimental Investigation on Flameholding Mechanism and Combustion Performance in Hydrogen-Fueled Supersonic Combustors," *Combustion Science and Technology*, Vol. 174, No. 3, 2002, pp. 1–27.

[7]Yu, G., Li, J. G., Zhang, X. Y., and Chen, L. H., "Investigation of Kerosene Combustion Characteristics with Pilot Hydrogen in Model Supersonic Combustors," *Journal of Propulsion and Power*, Vol. 17, No. 6, 2001, pp. 1263–1272.

[8]Kim, K. M., Baek, S. W., and Han, C. Y., "Numerical Study on Supersonic Combustion with Cavity Based Fuel Injection," *International Journal of Heat and Mass Transfer*, Vol. 47, No. 2, 2004, pp. 271–286.

[9]Rodriguez, C. G., and Cutler, A. D., "Numerical Analysis of the SCHOLAR Supersonic Combustor," NASA-CR-2003-212689, Dec. 2003.

[10]Oevermann, M., "Numerical Investigation of Turbulent Hydrogen Combustion in a SCRAMJET Using Flamelet Modeling," *Aerospace Science and Technology*, Vol. 4, Oct. 2000, pp. 463–480.

[11]FLUENT 6.1.18 User's Guide, Fluent, Inc., Lebanon, NH, Dec. 2003.

[12]Baurle, R. A., "Modeling of High Speed Reacting Flows: Established Practices and Future Challenges," AIAA Paper 2004-0267, April 2004.

[13]Baurle, R. A., and Eklund, D. R., "Analysis of Dual-Mode Hydrocarbon Scramjet Operation at Mach 4–6.5," *Journal of Propulsion and Power*, Vol. 18, No. 5, 2002, pp. 990–1002.

[14]Hsu, K., and Jemcov, A., "Numerical Investigation of Detonation in Pre-Mixed H_2-Air Mixture—Assesment of Simplified Chemical Mechanism," AIAA Paper 2000-2478, 2000.

[15]Baurle, R. A., Mathur, T., Gruber, M. R., and Jackson, K. R., "A Numerical and Experimental Investigation of a Scramjet Combustor for Hypersonic Missile Applications," AIAA Paper 1998-3121, 1998.

[16]von Lavante, E., Zeitz, D., and Kallenberg, M., "Numerical Simulation of Supersonic Airflow with Transverse Hydrogen Injection," *Journal of Propulsion and Power*, Vol. 17, No. 6, 2001, pp. 1319–1326.

[17]Pellett, G. L., Bruno, C., and Chinitz, W., "Review of Air Vitiation Effects on Scramjet Ignition and Flameholding Combustion Processes," AIAA Paper 2002-3880, July 2002.